ARTICLE

Li(V$_{0.5}$Ti$_{0.5}$)S$_2$ as a 1 V lithium intercalation electrode

Steve J. Clark[1,*], Da Wang[1,*], A. Robert Armstrong[2] & Peter G. Bruce[1]

Graphite, the dominant anode in rechargeable lithium batteries, operates at ∼0.1 V versus Li$^+$/Li and can result in lithium plating on the graphite surface, raising safety concerns. Titanates, for example, Li$_4$Ti$_5$O$_{12}$, intercalate lithium at ∼1.6 V versus Li$^+$/Li, avoiding problematic lithium plating at the expense of reduced cell voltage. There is interest in 1 V anodes, as this voltage is sufficiently high to avoid lithium plating while not significantly reducing cell potential. The sulfides, LiVS$_2$ and LiTiS$_2$, have been investigated as possible 1 V intercalation electrodes but suffer from capacity fading, large 1st cycle irreversible capacity or polarization. Here we report that the 50/50 solid solution, Li$_{1+x}$(V$_{0.5}$Ti$_{0.5}$)S$_2$, delivers a reversible capacity to store charge of 220 mAhg^{-1} (at 0.9 V), 99% of theoretical, at a rate of C/2, retaining 205 mAhg^{-1} at C-rate (92% of theoretical). Rate capability is excellent with 200 mAhg^{-1} at 3C. C-rate is discharge in 1 h. Polarization is low, 100 mV at C/2. To the best of our knowledge, the properties/performances of Li(V$_{0.5}$Ti$_{0.5}$)S$_2$ exceed all previous 1 V electrodes.

[1] Departments of Materials and Chemistry, University of Oxford, Parks Road, Oxford OX1 3PH, UK. [2] School of Chemistry and EastChem, University of St Andrews, North Haugh, Fife, Saint Andrews KY16 9ST, UK. * These authors contributed equally to this work. Correspondence and requests for materials should be addressed to P.G.B. (email: peter.bruce@materials.ox.ac.uk).

In order to avoid the potential danger of Li plating[1,2] on the widely used graphite anodes[3–5] in Li-ion batteries, which intercalate Li at 0.1 V versus Li^+/Li, important efforts have been made to identify anodes operating at 1 V (refs 6–9), including organic intercalation compounds[10] and conversion reactions[11,12]. In the former case, the low density inherent in molecular intercalation electrodes (typically $\sim 1.6\,g\,cm^{-3}$) (ref. 13) leads to low volumetric capacities. Volumetric energy density is an important parameter for future Li-ion batteries. The majority of conversion reactions exhibit large polarization (often in excess of 1 V), and voltages above 1 V on Li removal (discharge when used as an anode) are observed frequently[7,14]. In contrast, inorganic intercalation electrodes operate by a well-established mechanism, without the drastic changes that accompany conversion reactions, without involving nanoparticles and with higher densities than organic intercalation compounds.

Li can be intercalated into the layered compound $LiVO_2$ (cubic close packed structure) but at the very low voltage of <0.1 V (refs 15–17). In contrast, Li intercalation into the early transition metal sulfides, $LiMS_2$, M = V, Ti, occurs in the region of 1 V ($M^{2+/3+}$) and these materials have been explored previously, in pioneering studies, as possible anodes for Li-ion batteries[18–20].

However, previous work on $LiVS_2$ has shown that following Li intercalation, the subsequent Li extraction (corresponding to discharge when the $LiVS_2$ is used as an anode in a Li-ion battery) occurs at 1.3 V even at low rates and increases further with rate[18,20]. $LiVS_2$ is therefore not a true 1 V anode. Li intercalation into $LiTiS_2$ occurs at a lower voltage of 0.5 V, and exhibits very poor capacity retention on cycling, the capacity reducing to only $120\,mAhg^{-1}$ after just five cycles. $LiTiS_2$ also exhibits a massive 1st cycle irreversible loss of capacity of over $180\,mAhg^{-1}$ (ref. 18). We investigate the complete solid solution range $Li(V_{1-x}Ti_x)S_2$ and find that the 50/50 composition $Li(V_{0.5}Ti_{0.5})S_2$ delivers a significant improvement in properties/performance over other compositions, including the end members. A total of 50% replacement of V by Ti is sufficient to lower the potential (by lowering the Fermi level in the d-states) even on deintercalation (charge) below 1 V (0.9 V), but not to the extent of $LiTiS_2$ (where the consequence is massive irreversible capacity loss). The irreversible loss of capacity for $Li(V_{0.5}Ti_{0.5})S_2$ on the 1st cycle is only $42\,mAhg^{-1}$ at C/2 (compared with $180\,mAhg^{-1}$ for $LiTiS_2$). Furthermore, the polarization on the first cycle is half that of $LiVS_2$ at the same rate. $Li(V_{0.5}Ti_{0.5})S_2$ exhibits a reversible capacity of $220\,mAhg^{-1}$ at C/2 (99% of the theoretical capacity) dropping only marginally to $200\,mAhg^{-1}$ at 3C. The point of the paper is not to claim that the $Li(V_{0.5}Ti_{0.5})S_2$ material reported here is a commercially viable anode, with all practical problems solved. Rather it is to show that $LiMS_2$ based electrodes are not limited to the relatively poor performance (drastic capacity fading, large 1st cycle irreversible capacity and large polarization) reported previously and that sulfide based electrodes may merit further exploration in the future.

Results

$Li(V_{1-x}Ti_x)S_2$ solid solution. The range of compositions across the $Li(V_{1-x}Ti_x)S_2$ solid solution were synthesized as described in the Methods section, where the electrode fabrication and characterization methods are also described. The powder X-ray diffraction patterns are shown in Fig. 1a and correspond to the $LiMS_2$ structure, composed of hexagonal close packed S^{2-} with alternate sheets of octahedral sites occupied by Li and M cations, Fig. 1b. A comparison of powder X-ray patterns for $Li(V_{0.5}Ti_{0.5})S_2$ and the blend of 50 wt% $LiVS_2$ and 50 wt% $LiTiS_2$ is shown in Supplementary Fig. 1, confirming that the solid solution has been successfully synthesized. Li intercalation into this structure would require Li^+-occupying tetrahedral sites that share faces with Li in octahedral sites, and is therefore energetically unfavourable. Instead, upon intercalation, all the Li^+ ions in the octahedral sites in $LiMS_2$ are displaced to the neighboring tetrahedral sites in the alkali metal layers, as there are twice as many tetrahedral as octahedral sites the intercalating Li can be incorporated up to a theoretical maximum of Li_2MS_2 (ref. 18).

$Li(V_{0.5}Ti_{0.5})S_2$ was found to be the best performing of all the $Li(V_{1-x}Ti_x)S_2$ materials. Materials with more vanadium displayed increased polarization and deintercalation takes place above 1 V, comparisons with $Li(V_{0.6}Ti_{0.4})S_2$ and $LiVS_2$ are presented in Fig. 2a,b. Increasing the titanium content beyond 50% results in a decrease in capacity and increase in irreversible capacity on the 1st cycle, as is demonstrated by the $Li(V_{0.4}Ti_{0.6})S_2$ and $LiTiS_2$ data in Fig. 2c,d.

The electrochemical properties of $Li(V_{0.5}Ti_{0.5})S_2$. The charge–discharge curves for $Li(V_{0.5}Ti_{0.5})S_2$ are shown in Fig. 3. The capacity on cycling is $220\,mAhg^{-1}$ (2nd cycle) with the plateau on deintercalation (corresponding to the potential of ;the anode on discharge in a Li-ion cell) being located at 0.9 V. The polarization (separation between discharge and charge plateaus) is small, $\sim 100\,mV$ (rate = C/2). The load curves are invariant on subsequent cycling, save for a slow reduction in capacity. Concerning the first cycle, there is an initial capacity of $20\,mAhg^{-1}$ at ~ 2.1 V, associated with the $M^{4+/3+}$ redox couple and consistent with a small degree of lithium deficiency in the as-prepared material, $Li_{0.92}(V_{0.5}Ti_{0.5})S_2$, see refinement of structure, Supplementary Table 1. The main difference between the 1st and subsequent cycles is an additional, irreversible, capacity of $\sim 40\,mAhg^{-1}$ on cycle 1, Fig. 3, and is associated with reduction
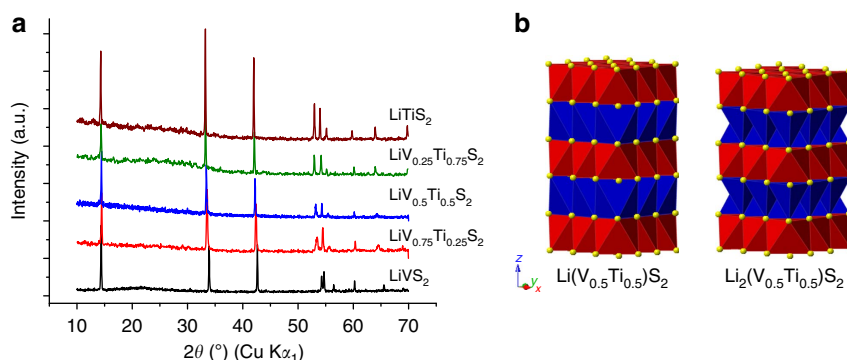

Figure 1 | Structures of $Li(V_{1-x}Ti_x)S_2$ and $Li_2(V_{0.5}Ti_{0.5})S_2$. (**a**) Powder X-ray diffraction patterns of as-prepared $Li(V_{1-x}Ti_x)S_2$. (**b**) Crystal structures of $Li(V_{0.5}Ti_{0.5})S_2$ and $Li_2(V_{0.5}Ti_{0.5})S_2$. Red octahedra—MS_6, blue polyhedra—LiS_x and yellow spheres—sulfur.
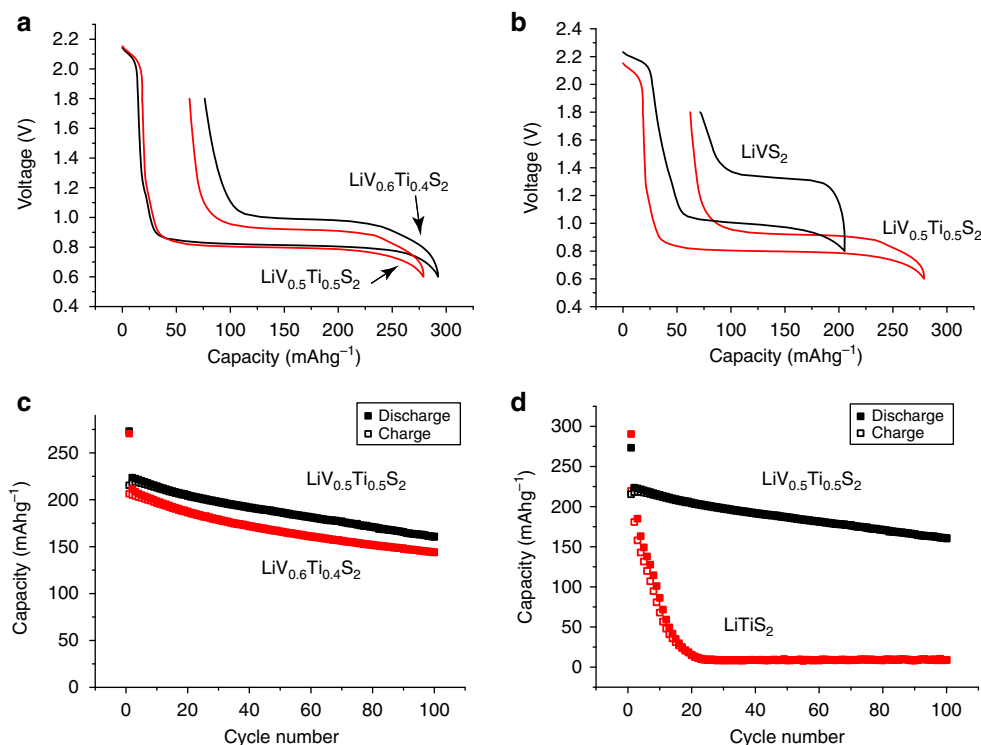
Figure 2 | Comparisons between Li(V$_{0.5}$Ti$_{0.5}$)S$_2$ and other members of the Li(V$_{1-x}$Ti$_x$)S$_2$ solid solution. (**a**,**b**) show the variation of potential with state-of-charge on the 1st cycle for Li(V$_{0.5}$Ti$_{0.5}$)S$_2$ and Li(V$_{0.6}$Ti$_{0.4}$)S$_2$, and LiVS$_2$ respectively. (**c**,**d**) show the variation of capacity with cycle number for Li(V$_{0.5}$Ti$_{0.5}$)S$_2$ and Li(V$_{0.4}$Ti$_{0.6}$)S$_2$, and LiTiS$_2$ respectively, Closed squares correspond to intercalation and open squares to deintercalation. All data were collected at a rate of 100 mAg^{-1}.

of the electrolyte. Electrolyte reduction/solid electrolyte interphase (SEI) layer formation has been observed previously for LiVS$_2$ and LiTiS$_2$ (ref. 18) and is discussed later for Li(V$_{0.5}$Ti$_{0.5}$) S$_2$.

The capacity as a function of cycle number for several different rates is shown in Fig. 4. The capacity on cycling is well maintained with increasing rate, for example, dropping by only 6% on increasing the rate from C/2 to 3C at cycle 10. The capacities on intercalation/de-intercalation during the first few cycles are affected by the irreversible capacity (on cycle 1) and at higher rates by an increase in capacity on cycling, something not infrequently seen in intercalation electrodes at high rates and often related to changes in the composite electrode structure within the first few cycles[21,22]. After the irreversible capacity loss on cycle 1, the charge/discharge efficiency improves rapidly over the first few cycles at all rates, Fig. 4. Overall the capacity retention on cycling after the first few cycles corresponds to a loss of ∼ 0.6 mAhg^{-1} per cycle. The origin of the capacity fading on cycling lies in the SEI layer formation and is discussed below.

The mechanism of intercalation into Li(V$_{0.5}$Ti$_{0.5}$)S$_2$. Given the change in properties/performance exhibited by the Li(V$_{0.5}$Ti$_{0.5}$)S$_2$ solid solution compared with the stoichiometric LiVS$_2$ and LiTiS$_2$ end members, it is important to ascertain if lithium intercalation into Li(V$_{0.5}$Ti$_{0.5}$)S$_2$ operates by the same mechanism. The results below show that the improved properties of Li(V$_{0.5}$Ti$_{0.5}$)S$_2$, are obtained despite a similar two-phase intercalation process and all three materials forming a SEI layer due to electrolyte degradation. Considering the structure of Li(V$_{0.5}$Ti$_{0.5}$)S$_2$ and its evolution on intercalation/deintercalation and cycling, joint refinements were carried out on the as-prepared material using the powder X-ray diffraction data in Supplementary Fig. 2 and the neutron diffraction data in Supplementary Fig. 3. Refined parameters are

given in Supplementary Table 1. The refined composition, Li$_{0.92}$(V$_{0.5}$Ti$_{0.5}$)S$_2$ is in good agreement with the capacity associated with the intercalation at 2.1 V (0.08 Li corresponds to 18 mAhg^{-1}). There is no evidence of site exchange between Li and V/Ti, that is, the structure remains layered, and no evidence of V/Ti long-range order. The V/Ti ratio refined to 1:1 within errors. The variation of structure with Li insertion/removal is shown in Fig. 5. The diffraction patterns were collected at the points on the load curve shown in Fig. 3. Initially, on intercalation Li fills the vacant octahedral sites in the Li layers of the as-prepared Li$_{0.92}$(V$_{0.5}$Ti$_{0.5}$)S$_2$, accounting for the first 18–20 mAhg^{-1} (between A and B in Fig. 3), this results in an expansion in a and c, from $a = 3.4247(1)$ Å and $c = 6.1582(2)$ Å to $a = 3.4377(4)$ Å and $c = 6.1591(2)$ Å. There is no change in the diffraction patterns between points B and C. Thereafter, Li intercalation is a 2-phase process, in accord with the plateau in Fig. 3, in which the as-prepared phase, Li(V$_{0.5}$Ti$_{0.5}$)S$_2$ is replaced continuously by Li$_2$(V$_{0.5}$Ti$_{0.5}$)S$_2$. On lithium extraction the 2-phase process is reversed, associated with the plateau on charge, as seen at point I in Fig. 3. Two phase refinements at points D–G and at I are well described by a mixture of the two end members with the compositions Li(V$_{0.5}$Ti$_{0.5}$)S$_2$ and Li$_2$(V$_{0.5}$Ti$_{0.5}$)S$_2$ and the patterns at A, B, C, H and J by single phases of the two end members. A cyclic voltammogram collected on a 3-electrode cell with the Li(V$_{0.5}$Ti$_{0.5}$)S$_2$ as the working electrode is shown in Supplementary Fig. 4 and exhibits one oxidation peak around 1 V and one reduction peak at 0.7 V, its shape is consistent with a 2-phase process, in accord with the powder X-ray diffraction results[23]. The above results show that the mechanism of Li intercalation into Li(V$_{0.5}$Ti$_{0.5}$)S$_2$ is essentially similar to that of LiVS$_2$ (ref. 18).

The refined a and c lattice parameters for Li$_1$(V$_{0.5}$Ti$_{0.5}$)S$_2$ and Li$_2$(V$_{0.5}$Ti$_{0.5}$)S$_2$ are respectively $a = 3.4377(4)$ Å, $c = 6.1591(2)$ Å
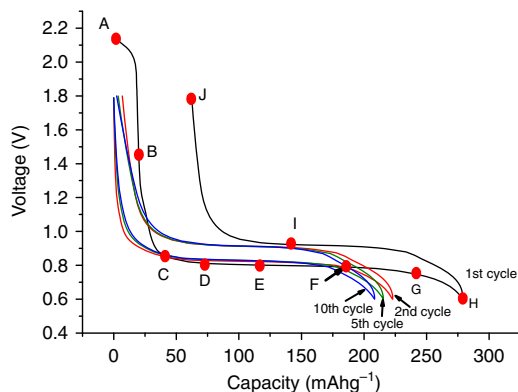
Figure 3 | Variation of potential (versus Li⁺/Li) with state of charge for Li(V$_{0.5}$Ti$_{0.5}$)S$_2$. Rate 100 mAg^{-1}. Letters correspond to various states of charge on the 1st cycle, see also Fig. 5.

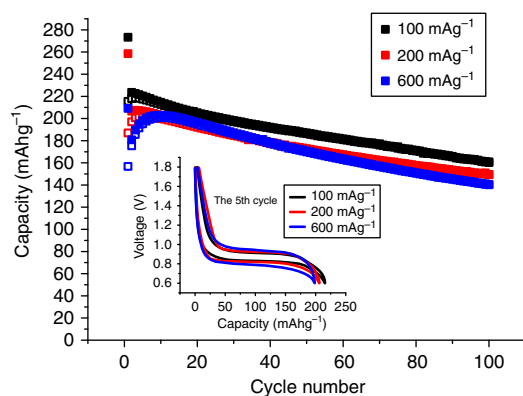**Figure 5 | Powder X-ray diffraction patterns of Li(V$_{0.5}$Ti$_{0.5}$)S$_2$ at various states of intercalation and deintercalation.** Letters correspond to points on the 1st cycle in Fig. 3. Highlighted regions show the presence of Li$_2$(V$_{0.5}$Ti$_{0.5}$)S$_2$ phase.

Figure 4 | Variation of capacity with cycle number for Li(V$_{0.5}$Ti$_{0.5}$)S$_2$. Closed squares correspond to intercalation and open squares to deintercalation. Inset shows load curves as a function of rate on the 5th cycle.

Figure 6 | SEM images. (**a**) Pressed pristine Li(V$_{0.5}$Ti$_{0.5}$)S$_2$ electrode and (**b**) Li(V$_{0.5}$Ti$_{0.5}$)S$_2$ electrode after 5 cycles. (**c**) Pristine Li(V$_{0.5}$Ti$_{0.5}$)S$_2$ electrode and (**d**) Li(V$_{0.5}$Ti$_{0.5}$)S$_2$ electrode after 1st discharge (intercalation) showing SEI layer formation on the surface of the electrode. Scale bar, (**a**,**b**) 10 μm, (**c**,**d**) 1 μm.

and $\boldsymbol{a} = 3.7894(7)$ Å, $\boldsymbol{c} = 6.229(2)$ Å. The volume expansion on intercalation is 23% yet the phase transformation is facile. The expansion along $\boldsymbol{a}$ is associated with the elongation of the (Ti/V)-S bond as formally (Ti/V)$^{3+}$ is reduced to (Ti/V)$^{2+}$. As the d-bands in sulfides are relatively wide compared with oxides, the electrons are well delocalized across the (Ti/V)-S$_2$ slabs. The c-axis expansion requires energy to increase the separation of the slabs. The small c-axis expansion, only 1.5%, may be responsible for the facile nature of the 2-phase intercalation reaction that exhibits a small polarization and excellent reversibility. Powder X-ray diffraction (PXRD) data collected on cycling, Supplementary Fig. 5 shows that the 2-phase intercalation/de-intercalation mechanism continues to operate. There is no change in lattice parameters with cycling. SEM images of electrodes were collected before and after cycling, Fig. 6a,b. The average particle size of Li(V$_{0.5}$Ti$_{0.5}$)S$_2$ is 20 μm and remains so on cycling. All of these results indicate that the material is stable on cycling.

SEI layer formation and capacity fade. Electrolyte reduction and SEI layer formation have been reported for LiVS$_2$ and LiTiS$_2$, where it was inferred only from the electrochemistry[18]. Of the ~40 mAg^{-1} of irreversible capacity on the first cycle for Li(V$_{0.5}$Ti$_{0.5}$)S$_2$, Fig. 3, the 20 mAg^{-1} of capacity between B and C may be assigned to electrolyte reduction, as there is no change
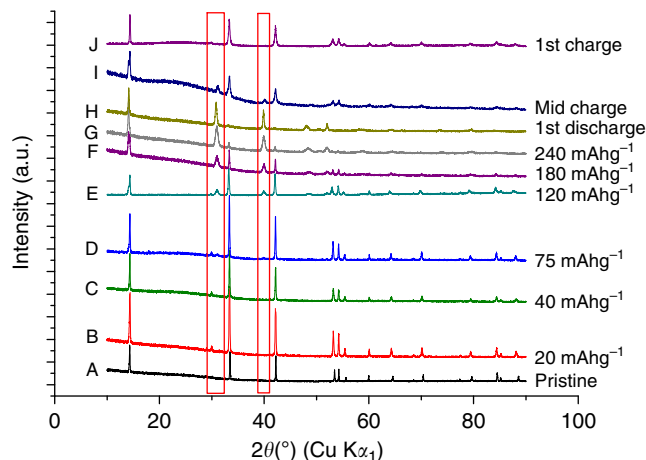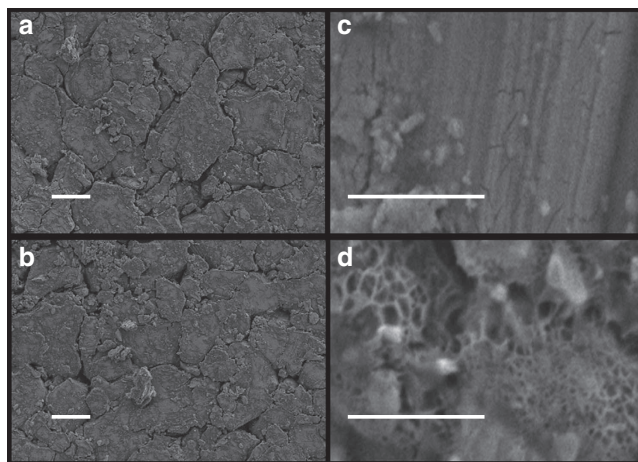
in the lattice parameters. Beyond C, the Rietveld refinements of the 2-phase mixtures of Li(V$_{0.5}$Ti$_{0.5}$)S$_2$ and Li$_2$(V$_{0.5}$Ti$_{0.5}$)S$_2$ along the plateau provide the ratios of the two phases, which in turn gives the amount of lithium and hence charge that has been inserted into the structure. These values are presented in Table 1 along with the values for the total charge passed minus the 20 mAg^{-1} at the beginning of discharge associated with the M$^{4+/3+}$ redox couple. There is almost no difference in these values across the plateau, indicating that no significant electrolyte reduction occurs between C and G in Fig. 3. The remainder of the electrolyte reduction occurs beyond point G, in accord with the slow downturn in the potential. Extending the cut-off potential to lower values increases this electrolyte reduction and hence irreversible capacity significantly, which is why lower voltage anodes are less attractive. The amount of true intercalation capacity derived from the refinement of the PXRD data is consistent with the theoretical capacity for Li(V$_{0.5}$Ti$_{0.5}$)S$_2$ (222 mAg^{-1}) and the observed capacity on the 2nd cycle,

Point	Capacity from load curve minus the $M^{4+/3+}$ couple ($mAhg^{-1}$)	Capacity of Li intercalated into $Li(V_{0.5}Ti_{0.5})S_2$ from X-ray analysis ($mAhg^{-1}$)	Difference ($mAhg^{-1}$)
B	0	0	0
C	20	0	20
D	50	28	22
E	95	72	23
F	155	133	22
G	215	195	20
H	258	216	42

Table 1 | Comparison between capacity observed electrochemically and intercalated capacity derived from X-ray refinements.

Letters correspond to the points on the 1st cycle in Fig. 3.

Figure 7 | AC impedance spectra. AC impedance of the $Li(V_{0.5}Ti_{0.5})S_2$/ electrolyte interface collected at the end of the 1st, 10th, 50th and 100th cycles using 3-electrode cells.

Fig. 3. This demonstrates that the additional (irreversible) capacity on cycle 1 is due primarily to electrolyte reduction.

It is important to recall that the composite electrodes contain 10% super S carbon, and this will account for some of the observed electrolyte reduction (irreversible capacity). Cells were constructed with the same loading of $Li(V_{0.5}Ti_{0.5})S_2$ per unit area as in Fig. 3, but without super S carbon, the comparison between the two cells is shown in Supplementary Fig. 6. The load curve without super S shows virtually no capacity between 0.93 and 1.3 V, suggesting that the $\sim 12\,mAhg^{-1}$ loss observed between those voltages for the electrode containing Super S is associated with electrolyte reduction on the carbon surface. The capacity between 0.93 V and point C, $8\,mAhg^{-1}$, could be due to reduction of the electrolyte on the surface of $Li(V_{0.5}Ti_{0.5})S_2$ as it is present in the electrode with and without carbon. It might also arise from a very small amount of intercalation, corresponding to $x = 0.03$, too small to be seen in the X-ray data. The irreversible capacity loss occurring at the lower voltage beyond the plateau, <0.7 V, appears also due to a combination of carbon and $Li(V_{0.5}Ti_{0.5})S_2$, since it increases when super S is present. Overall, Supplementary Fig. 6 shows that of the irreversible capacity observed in Fig. 3, only $25\,mAhg^{-1}$ arises from electrolyte reduction on the $Li(V_{0.5}Ti_{0.5})S_2$ surface that is, 11% of the reversible capacity, the rest is due to reduction on the surface of the super S.

To explore the SEI layer formation as a function of cycling, alternating current (AC) impedance spectroscopy and SEM (scanning electron microscopy) images were collected from cycles 1 to 100, Figs 7 and 8. The AC impedance data, from 3-electrode cells, show two semicircles, as is typical for the electrode/electrolyte interface[24]. The interfacial impedance grows continuously with cycle number indicative of a growing SEI layer. This was confirmed by examination of the SEM images, Fig. 8, where the SEI layer is seen to grow on the electrode particles from several nanometers at cycle 10 up to $>1\,\mu m$ at cycle 100. The growing SEI layer is consistent with the capacity fading observed on cycling. Confirmation that the capacity fading is not intrinsic to the material but is due to the SEI layer growth was provided by the powder X-ray diffraction patterns at the 25th cycle, Supplementary Fig. 5, which showed the crystal structure is preserved and the 2-phase reaction remains on cycling. We have used standard LP30 electrolyte, but this is optimized for graphite and not for sulfide electrodes operating near 1 V. A detailed investigation of alternative electrolytes, electrolyte additives and of surface coatings on the sulfide may be able to reduce further the irreversible capacity on the 1st cycle even below the 11% associated with reduction on the $Li(V_{0.5}Ti_{0.5})S_2$ itself, and to reduce significantly the capacity fading on cycling.

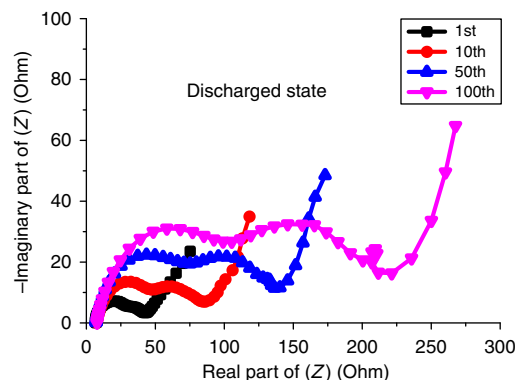**$Li(V_{0.5}Ti_{0.5})S_2$ in a full lithium-ion cell**. $Li(V_{0.5}Ti_{0.5})S_2$ was incorporated as the anode in a full lithium-ion cell with a $LiCoO_2$ cathode. The cell was constructed such that the overall capacity was anode limited, in order to show the performance of the latter, see Methods section. First charge capacity, corresponding to insertion of lithium into $Li(V_{0.5}Ti_{0.5})S_2$, exhibits a larger irreversible capacity than was observed when the counter electrode was lithium metal ($\sim 75\,mAhg^{-1}$ as opposed to $42\,mAhg^{-1}$), see Fig. 9. In full cells the anode potential can reach lower values on charge than is the case for a lithium counter electrode. If this happens there will be a higher irreversible capacity, as observed here. The overall capacity on the first charge in Fig. 9 is $310\,mAhg^{-1}$ compared with $278\,mAhg^{-1}$ for the cell with a Li counter electrode, the difference is the same as the additional irreversible capacity ($75–42\,mAhg^{-1}$), consistent with the additional irreversible capacity in Fig. 9. Lowering the voltage cutoff below 3.4 V seen in Fig. 9 leads to a loss of reversible capacity on the first and subsequent cycles. The discharge capacity is $\sim 215\,mAhg^{-1}$, just below the theoretical capacity; this reduces to just over $180\,mAhg^{-1}$ by the 10th cycle, see Supplementary Fig. 7. The purpose of this experiment was simply to show that a full cell can be constructed and cycled using the new anode.

Sulfides are used in a variety of applications ranging from pigments[25] to solar cells[26], they are not exotic materials. Although the sulfides here are synthesized in sealed tubes for convenience in the lab, this is not ubiquitous for sulfides, other methods can be used[27,28]. V is not the lowest cost element but several V based electrodes are under investigation and have been reported, for example, V_2O_5, Na_xVO_2, $LiVO_2$, and of course V redox-flow batteries are in use and continue to be studied[15,29–31]. The materials we report showed no change in their powder X-ray diffraction patterns after 12 h exposure to ambient air, Supplementary Fig. 8. After 15 h a small peak begins to appear at 11° in 2θ, Supplementary Fig. 8 and grows with time, showing that the sulfides are air sensitive as expected. The widely used $LiFePO_4$ cathode material is also not stable in air and is packed in sealed containers after synthesis for shipping. A similar approach could be taken with $Li(V_{0.5}Ti_{0.5})S_2$. We suggest that the relatively slow rate of reaction in air is likely due to the formation of a thin oxide layer that slows decomposition.

Discussion

An intercalation anode, $Li(V_{0.5}Ti_{0.5})S_2$, is reported that operates at 0.9 V versus Li^+/Li (56% lower voltage than $Li_4Ti_5O_{12}$

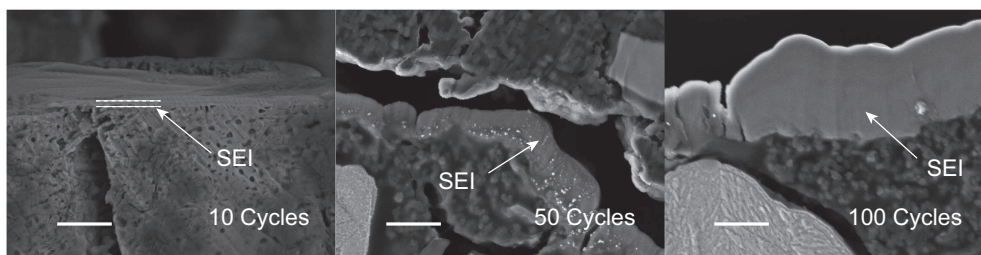**Figure 8 | Cross-sectional SEM images.** Cross-sectional SEM images of the $Li(V_{0.5}Ti_{0.5})S_2$ electrode collected at the end of the 10th, 50th and 100th cycles. Scale bar, 1 µm.
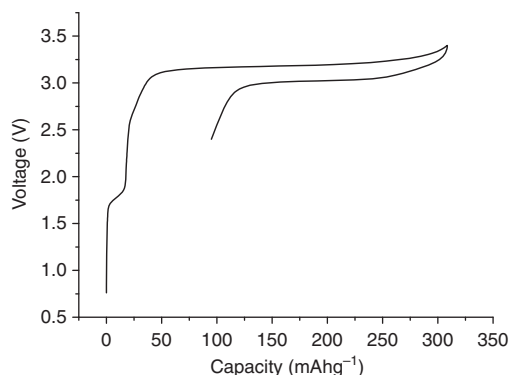

Figure 9 | Variation of potential with state of charge for the $Li(V_{0.5}Ti_{0.5})S_2/LiCoO_2$ cell. Rate 100 mAg^{-1} of anode, cells were cycled between 3.4 V and 2.4 V.

refs 32–34), with low polarization, 100 mV, a capacity of 220 mAhg^{-1} at C/2 on cycling, corresponding to 99% of theoretical capacity, good rate capability, 205 mAhg^{-1} at 1C and 200 mAhg^{-1} at 3C. The volumetric capacity is 740 mAhcm^{-3}, comparable to the reversible volumetric capacity of graphite (600–700 mAh cm^{-3})[35], but at a potential (0.9 V) that avoids Li plating. As such, this material delivers significantly better properties/performance than the previously studied end-members, LiVS$_2$ (the voltage of which is >1 V versus Li$^+$/Li) and LiTiS$_2$ (which exhibits a very large irreversible capacity loss on the 1st cycle of 180 mAhg^{-1}). Electrolyte reduction on $Li(V_{0.5}Ti_{0.5})S_2$ during the first cycle accounts for only 11% of the first cycle capacity. Performance is better than previously reported 1 V anodes, to the best of our knowledge. Future work should focus on reducing the 1st cycle irreversible capacity while forming a robust SEI layer minimizing further electrolyte reduction, by examining lowering the amount of conductive additive in the electrode and investigating electrolyte additives or seeking alternative electrolytes to those optimized for graphite anodes.

Methods

Synthesis. $Li(V_{0.5}Ti_{0.5})S_2$ was synthesized from Li$_2$S (Aldrich, 99.9%), Ti powder (Aldrich, 99.98%), V powder (Aldrich, 99.5%) and S powder (Aldrich, 99.98%). Appropriate ratios of starting materials were mixed and ground together in an Ar filled MBraun glovebox. The mixture was then placed in a graphite crucible, which was in turn placed in a quartz tube. The quartz tube was subsequently sealed under vacuum. The reactants were heated at 1,050 °C for 72 h before being quenched to room temperature.

Electrochemical measurements. Composite electrodes were fabricated using the active material, super S carbon and Kynar Flex 2801 (a co-polymer based on polyvinylidene difluoride) binder in a mass ratio of 80:10:10. The mixture was then cast on copper foil using tetrahydrofuran as the solvent. The loading of active material was ∼6–8 mg cm^{-2}. Electrochemical cells consisting of a $Li(V_{0.5}Ti_{0.5})S_2$ composite electrode, a lithium metal counter electrode and a glass microfiber GF/F

separator (WhatmanTM) saturated with electrolyte, a 1 M solution of LiPF$_6$ in ethylene carbonate–dimethyl carbonate 1:1 ((v/v) (BASF)), were constructed. Li-ion cells were constructed similarly with composite LiCoO$_2$ electrodes (LiCoO$_2$, Super S and Kynar Flex 2801 in a mass ratio of 80:10:10) replacing the lithium metal counter. Celgard monolayer polypropylene separator was used in addition to the glass microfiber separator. All handling was carried out in an Ar filled MBraun glovebox. Electrochemical measurements were conducted using a Maccor series 4,200 battery tester. Cyclic voltammetry and AC impedance were conducted on 3-electrode cells using a VMP3 electrochemical workstation (Biologic).

Structural analysis. Powder X-ray diffraction patterns were obtained using a Stoe STADI/P diffractometer employing CuKα$_1$ radiation operating in transmission mode with the samples sealed in 0.2 mm capillaries, expect for the experiments on air sensitivity, which were carried out in air. Time-of-flight powder neutron diffraction data were collected on the POLARIS high-intensity; medium resolution instrument at ISIS, Rutherford Appleton Laboratory (UK) with samples sealed in 2 mm quartz capillaries. The structures were refined by the Rietveld method using TOPAS Academic[36]. Samples with different Li amounts for X-ray diffraction were prepared electrochemically. After cycling, cells were transferred to an argon-filled glove box before opening and active material removed. The electrodes were then rinsed with a small amount of dry dimethyl carbonate to remove residual electrolyte. They were left under dynamic vacuum overnight to ensure all solvent had evaporated before measurements were collected. SEM studies were carried out using a Carl Zeiss Merlin instrument. Electrodes for cross-sectional imaging were rotary-etched in a Gatan Precision Etching Coating System (PECS 682).

References

1. Smart, M. C. & Ratnakumar, B. V. Effects of electrolyte composition on lithium plating in lithium-ion cells. *J. Electrochem. Soc.* **158,** A379–A389 (2011).
2. Petzl, M., Kasper, M. & Danzer, M. A. Lithium plating in a commercial lithium-ion battery—a low-temperature aging study. *J. Power Sources* **275,** 799–807 (2015).
3. Armand, M. & Tarascon, J. M. Building better batteries. *Nature* **451,** 652–657 (2008).
4. Etacheri, V., Marom, R., Elazari, R., Salitra, G. & Aurbach, D. Challenges in the development of advanced Li-ion batteries: A review. *Energy Environ. Sci.* **4,** 3243–3262 (2011).
5. Noel, M. & Suryanarayanan, V. Role of carbon host lattices in li-ion intercalation/de-intercalation processes. *J. Power Sources* **111,** 193–209 (2002).
6. Oumellal, Y., Rougier, A., Nazri, G. A., Tarascon, J. M. & Aymard, L. Metal hyrides for lithium-ion batteries. *Nat. Mater.* **7,** 916–921 (2008).
7. Goriparti, S. *et al.* Review on recent progress of nanostructured anode materials for li-ion batteries. *J. Power Sources* **257,** 421–443 (2014).
8. Gao, H., Liu, C. L., Liu, Y., Liu, Z. H. & Dong, W. S. MoO$_2$-loaded porous carbon hollow spheres as anode materials for lithium-ion batteries. *Mater. Chem. Phys.* **147,** 218–224 (2014).
9. Goodenough, J. B. & Kim, Y. Challenges for rechargeable Li batteries. *Chem. Mater.* **22,** 587–603 (2010).
10. Armand, M. *et al.* Conjugated dicarboxylate anodes for Li-ion batteries. *Nat. Mater.* **8,** 120–125 (2009).
11. Cabana, J., Monconduit, L., Larcher, D. & Palacin, M. R. Beyond intercalation-based Li-ion batteries: The state of the art and challenges of electrode materials reacting through conversion reactions. *Adv. Mater.* **22,** E170–E192 (2010).
12. Zhang, L., Wu, H. B. & Lou, X. W. Iron-oxide-based advanced anode materials for lithium ion batteries. *Adv. Energy Mater.* **4,** 1300958 (2014).
13. Kaduk, J. A. Terephthalate salts: salts of monopositive cations. *Acta Crystallogr. B-Struct. Sci.* **56,** 474–485 (2000).
14. Park, G. D. & Kang, Y. C. Superior lithium-ion storage properties of mesoporous CuO-reduced graphene oxide composite powder prepared by a two-step spray-drying process. *Chem. Eur. J.* **21,** 9179–9184 (2015).
15. Armstrong, A. R., Lyness, C., Panchmatia, P. M., Islam, M. S. & Bruce, P. G. The lithium intercalation process in the low-voltage lithium battery anode Li$_{1+x}$V$_{1-x}$O$_2$. *Nat. Mater.* **10,** 223–229 (2011).

16. Choi, N. S., Kim, J. S., Yin, R. Z. & Kim, S. S. Electrochemical properties of lithium vanadium oxide as an anode material for lithium-ion battery. *Mater. Chem. Phys.* **116,** 603–606 (2009).

17. Pourpoint, F. *et al.* New insights into the crystal and electronic structures of $Li_{1+x}V_{1-x}O_2$ from solid state NMR, pair distribution function analyses, and first principles calculations. *Chem. Mater.* **24,** 2880–2893 (2012).

18. Kim, Y., Park, K. S., Song, S. H., Han, J. T. & Goodenough, J. B. Access to M^{3+}/M^{2+} redox couples in layered $LiMS_2$ sulfides ($M = Ti$, V, Cr) as anodes for Li-ion battery. *J. Electrochem. Soc.* **156,** A703–A708 (2009).

19. Murphy, D. W. & Carides, J. N. Low voltage behavior of lithium/metal dichalcogenide topochemical cells. *J. Electrochem. Soc.* **126,** 349–351 (1979).

20. Gupta, A., Mullins, C. B. & Goodenough, J. B. Electrochemical probings of $Li_{1+x}VS_2$. *Electrochim. Acta* **78,** 430–433 (2012).

21. Wei, X. *et al.* Electrochemical performance of high-capacity nanostructured $Li[Li_{0.2}Mn_{0.54}Ni_{0.13}Co_{0.13}]O_2$ cathode material for lithium ion battery by hydrothermal method. *Electrochim. Acta* **107,** 549–554 (2013).

22. Prosini, P. P., Zane, D. & Pasquali, M. Improved electrochemical performance of a $LiFePO_4$-based composite cathode. *Electrochim. Acta* **46,** 3517–3523 (2001).

23. Robertson, A. D., Tukamoto, H. & Irvine, J. T. S. $Li_{1+x}Fe_{1-3x}Ti_{1+2x}O_4$ ($0.0 \leq x \leq 0.33$) based spinels: possible negative electrode materials for future Li-ion batteries. *J. Electrochem. Soc.* **146,** 3958–3962 (1999).

24. Zhang, S. S., Xu, K. & Jow, T. R. EIS study on the formation of solid electrolyte interface in Li-ion battery. *Electrochim. Acta* **51,** 1636–1640 (2006).

25. Anglos, D. *et al.* Laser-induced fluorescence in artwork diagnostics: an application in pigment analysis. *Appl. Spectrosc.* **50,** 1331–1334 (1996).

26. Guo, Q. *et al.* Fabrication of 7.2% efficient CZTSSe solar cells using CZTS nanocrystals. *J. Am. Chem. Soc.* **132,** 17384–17386 (2010).

27. Murphy, D. W., Cros, C., Disalvo, F. J. & Waszczak, J. V. Preparation and properties of Li_xVS_2. *Inorg. Chem.* **16,** 3027–3031 (1977).

28. Vanlaar, B. & Ijdo, D. J. W. Preparation, crystal structure, and magnetic structure of $LiCrS_2$ and $LiVS_2$. *J. Solid State Chem.* **3,** 590–595 (1971).

29. Li, X. F., Zhang, H. M., Mai, Z. S., Zhang, H. Z. & Vankelecom, I. Ion exchange membranes for vanadium redox flow battery (VRB) applications. *Energy Environ. Sci.* **4,** 1147–1160 (2011).

30. Liu, Q. *et al.* Graphene-modified nanostructured vanadium pentoxide hybrids with extraordinary electrochemical performance for Li-ion batteries. *Nat. Commun.* **6,** 6127 (2015).

31. Guignard, M. *et al.* P2-Na_xVO_2 system as electrodes for batteries and electron-correlated materials. *Nat. Mater.* **12,** 74–80 (2013).

32. Ferg, E., Gummow, R. J., Dekock, A. & Thackeray, M. M. Spinel anodes for lithium-ion batteries. *J. Electrochem. Soc.* **141,** L147–L150 (1994).

33. Colbow, K. M., Dahn, J. R. & Haering, R. R. Structure and electrochemistry of the spinel oxides $LiTi_2O_4$ and $Li_{4/3}Ti_{5/3}O_4$. *J. Power Sources* **26,** 397–402 (1989).

34. Yang, Z. G. *et al.* Nanostructures and lithium electrochemical reactivity of lithium titanites and titanium oxides: a review. *J. Power Sources* **192,** 588–598 (2009).

35. Sivakkumar, S. R., Nerkar, J. Y. & Pandolfo, A. G. Rate capability of graphite materials as negative electrodes in lithium-ion capacitors. *Electrochim. Acta* **55,** 3330–3335 (2010).

36. Coelho, A. A. Whole-profile structure solution from powder diffraction data using simulated annealing. *J. Appl. Crystallogr.* **33,** 899–908 (2000).

Acknowledgements

Author contributions

S.J.C. and D.W. carried out experiments. A.R.A. carried out structural refinements. P.G.B. wrote the manuscript. All authors contributed to the discussion and interpretation of the results.

Additional information

Supplementary Information accompanies this paper at http://www.nature.com/naturecommunications

Competing financial interests: The authors declare no competing financial interests.

Reprints and permission information is available online at http://npg.nature.com/reprintsandpermissions/

How to cite this article: Clark, S. J. *et al.* $Li(V_{0.5}Ti_{0.5})S_2$ as a 1 V lithium intercalation electrode. *Nat. Commun.* 7:10898 doi: 10.1038/ncomms10898 (2016).